

Changes in density fluctuations associated with confinement transitions close to a rational edge rotational transform in the W7-AS stellarator

This article has been downloaded from IOPscience. Please scroll down to see the full text article.

2002 Plasma Phys. Control. Fusion 44 1581

(<http://iopscience.iop.org/0741-3335/44/8/311>)

View [the table of contents for this issue](#), or go to the [journal homepage](#) for more

Download details:

IP Address: 130.183.100.180

The article was downloaded on 28/05/2010 at 07:50

Please note that [terms and conditions apply](#).

Changes in density fluctuations associated with confinement transitions close to a rational edge rotational transform in the W7-AS stellarator

S Zoletnik^{1,6}, N P Basse^{2,4}, M Saffman³, W Svendsen^{2,4}, M Endler⁵,
M Hirsch⁵, A Werner⁵, Ch Fuchs⁵ and the W7-AS Team⁵

¹ CAT-SCIENCE Bt. Detrekő u. 1/b H-1022 Budapest, Hungary

² Optics and Fluid Dynamics Department, Risø National Laboratory, EURATOM Association, Roskilde DK-4000, Denmark

³ Department of Physics, University of Wisconsin, Madison, WI 53706, USA

⁴ Ørsted Laboratory, H C Ørsted Institute, Universitetsparken 5, Copenhagen DK-2100, Denmark

⁵ Max-Planck-Institut für Plasmaphysik, EURATOM Association, Garching D-85748, Germany

⁶ KFKI-RMKI, EURATOM Association, Budapest H-1125, Hungary

Received 8 April 2002

Published 22 July 2002

Online at stacks.iop.org/PPCF/44/1581

Abstract

At certain values of the edge rotational transform t_a , the confinement quality of plasmas in the Wendelstein 7-AS (W7-AS) stellarator is found to react very sensitively to small modifications of the edge rotational transform t_a . As t_a can be reproducibly changed either by external fields or by a small plasma current, these transitions offer a precise way to systematically analyse differences in plasma turbulence between bad and good confinement cases. This paper presents results of the study of electron density fluctuations associated with confinement changes. Wavenumber and frequency spectra and radial profiles are compared. A slow and reproducible transition is induced by a small plasma current and the sequence of events leading to bad confinement is investigated. The laser scattering core plasma density fluctuation measurements are complemented by edge beam emission spectroscopy results and magnetic fluctuation measurements with Mirnov coils.

Clear correspondence between plasma fluctuations and confinement degradation is observed: the weight of larger structures increases, fluctuations increase in the plasma core, the poloidal flow velocity decreases and regions of mode-like activity move radially in the plasma. These changes occur gradually and controllably if the magnetic configuration is steered by a small plasma current.

1. Introduction

A considerable amount of experimental evidence has been collected recently on various fusion devices that anomalous electron transport in both tokamaks and stellarators is strongly dependent on the safety factor q of the magnetic field. Strong local temperature and density

gradients were found in some tokamaks [1, 2] and heat transport showed local transport barriers in the vicinity of low-order rational surfaces [3]. In the Wendelstein 7-AS (W7-AS) stellarator [4], where the profile of the rotational transform ($t = 1/q$) as a function of the major radius is nearly flat, a strong dependency of the plasma confinement quality on the edge rotational transform (rotational transform at the last closed flux surface: t_a) was found. At certain rotational transform values the confinement quality, as measured by, for example, the plasma total energy content at fixed heating power and line averaged density, changes considerably [4]. A phenomenological model of the radial electron heat transport [5, 6] could reproduce this dependency by assuming that the heat diffusivity is considerably higher in the vicinity of rational surfaces if the magnetic shear in the plasma is low. This finding again points to the link between rational surfaces and anomalous plasma transport.

It is generally assumed that anomalous transport is caused by turbulence in the plasma [7, 8], although a consensus on the mechanism and the underlying instabilities has not been achieved yet. As the plasma turbulence should involve some kind of fluctuations in the plasma parameters, a considerable effort has been devoted to the measurement of plasma fluctuations especially in the plasma density and to lesser extent in the temperature and other plasma parameters. Although correspondence between the fluctuation amplitude and confinement quality was found in some cases [7, 8], changes in the fluctuation amplitude are not always correlated with confinement changes [9].

Given this unclear situation it would be important to analyse the behaviour of fluctuations in the case of controllable changes in the plasma confinement. The reproducibility and controllability of the confinement properties of plasma discharges in the W7-AS stellarator provide a perfect opportunity for this task. In the standard currentless operation, the magnetic field configuration is determined mostly by the externally applied fields. In contrast to tokamaks, the internal plasma currents give only a small contribution to the rotational transform profile. At certain edge rotational transform values the energy confinement time changes about a factor of 2 in response to about 5% change in t_a . Such a minor change can be achieved in two ways: either by changing the externally applied t or by a relatively small (<2 kA) Ohmic plasma current. Although the radial profile of the rotational transform is somewhat different in the two cases, experience shows that plasma confinement changes similarly. This way a controlled confinement transition can be performed from shot-to-shot or within one discharge by a small Ohmic plasma current.

This paper intends to give a detailed analysis of changes in electron density fluctuations during confinement degradation induced by modification of the externally applied rotational transform or by an internal Ohmic current. The two degraded cases are compared to each other and to the initial good confinement case. Density fluctuations were measured by the double-volume localized turbulence scattering (LOTUS) laser scattering diagnostic and complemented by edge beam emission spectroscopy (BES) fluctuation measurements. Some results from edge poloidal magnetic field measurements with Mirnov coils are also presented for comparison.

The paper is organized as follows. Section 2 describes the discharges used for the investigation and section 3 outlines the laser scattering diagnostic. Comparison of fluctuations in good and bad confinement plasmas are presented in section 4, while the transition is analysed in section 5. The results are discussed in section 6.

2. Description of plasma discharges

The discharges were done with $B_t = 2.5$ T toroidal and 22 mT vertical magnetic field and 400 kW electron cyclotron resonance heating (ECRH) at 140 GHz. The central electron density

was kept at $n_e(0) = 8 \times 10^{19} \text{ m}^{-3}$. The rotational transform at the plasma edge was set either to $t_a = 0.344$ ('good confinement') or to $t_a = 0.362$ ('bad confinement'). From the diamagnetically measured total energy content, the energy confinement time is estimated to be 22 and 12 ms in the good and bad confinement cases, respectively. In the first 400 ms of the discharge the plasma current was compensated to zero, while from 400 to 500 ms it was ramped up to 2 kA and then down to 0 at the same rate. Some diagnostic signals of two example discharges at the two t values are shown in figure 1.

Before 400 ms into the discharge, the two plasmas differ in many respects. Their temperature and, as a consequence, their diamagnetically measured total stored energy differ by about a factor of 2, indicating the difference in energy confinement time. The gas feed rate,

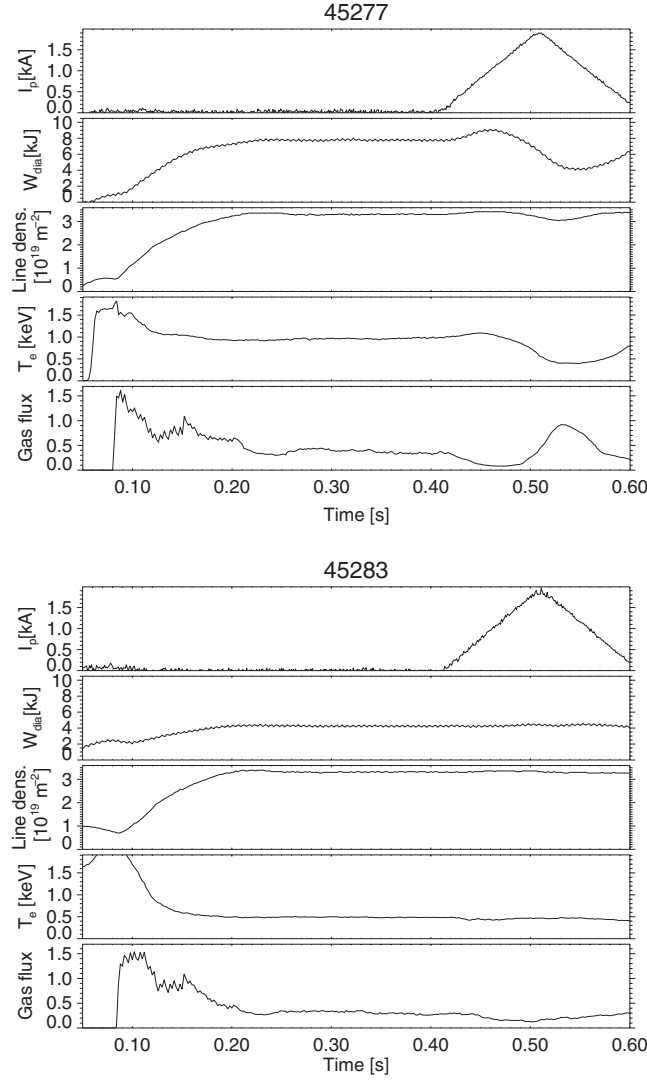


Figure 1. Some diagnostic signals of a 'good' (top) and a 'bad' (bottom) confinement discharge. From top to bottom: total plasma current, diamagnetically measured total stored energy, line integrated electron density, central T_e from ECE and gas influx rate.

which is needed to maintain the preprogrammed line integrated electron density, also differs considerably, indicating a difference in particle confinement time as well.

The effect of the current ramp can be understood by considering that the positive plasma current increases ι . The plasma current approximately changes the edge ι as 0.007 kA^{-1} [5]; this way the 2 kA current changes it from the ‘good’ 0.344 to 0.358, close to the ‘bad’ (0.362) ι . Consequently the plasma energy confinement decreases to the bad case. It is interesting to see that in response to the plasma current ramp, the energy content of the good confinement discharge reacts first with a moderate increase, *then* it starts to decrease gradually. The origin of this fast confinement improvement is not clear, but most probably it is caused by the fact that at zero net current the plasma was not exactly at the optimum confinement. The diamagnetic energy signal reaches a minimum somewhat after the peak of the plasma current then it increases again. As the discharge ends at about 600 ms, when the current reaches zero, the total energy does not recover to the initial value. (In some discharges the plasma was sustained for 100 ms after the current reached 0 and the plasma recovered its initial state.) Similarly to the diamagnetic signal the gas feed rate also changes during the current ramp indicating the change in particle confinement as well. The same current ramp in the bad confinement discharge does not cause substantial changes.

It is important to observe that unlike in the case of the L- to H-mode transition [10], where the transition takes place abruptly (on its own timescale) in shorter than 10 ms time, the present confinement change happens smoothly, the timescale depends on the current ramping rate. The response of the diamagnetic signal to the current ramp is nearly symmetric in time, but delayed relative to it. The delay can most probably be attributed to the current penetration time into the plasma; therefore this type of discharge cannot be used to analyse the transition itself. For this purpose another discharge type was used where the plasma current was ramped up to 2 kA in 700 ms time. However, in this case the discharge was not long enough to ramp the current back to 0 and analyse a possible hysteresis effect. An example for a slow current ramp discharge is shown in figure 2. It can be clearly observed that the plasma energy content drops continuously

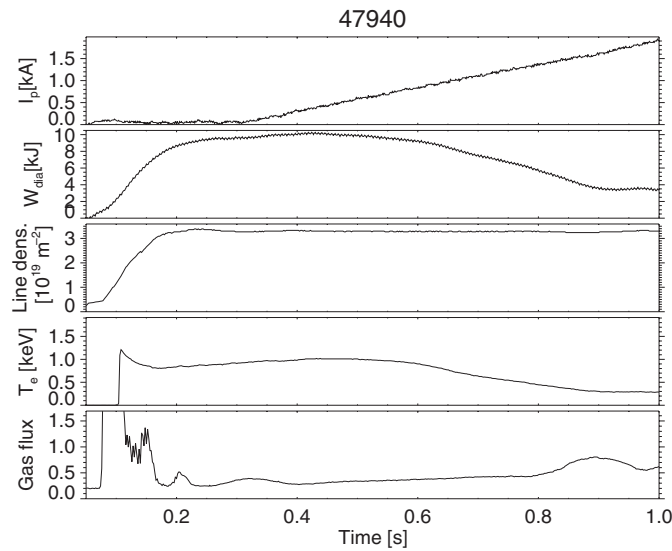


Figure 2. Some diagnostic signals of a ‘good’ confinement discharge with slow current ramp. From top to bottom: total plasma current, diamagnetically measured total stored energy, line integrated electron density, central T_e from ECE and gas influx rate.

in about 400 ms time. Two phases can be observed. In the first phase (before 0.79 s) the energy content and the gas feed rate changes slowly. In the second phase the slope of the diamagnetic signal drop increases by about a factor of 2 and the gas feed rate also changes faster. At 900 ms (1.7 kA), saturation is reached. This behaviour clearly shows that the confinement change analysed in this paper is not abrupt but can be smoothly controlled; positive feedback mechanisms are not expected. If the changes are caused by changes in the plasma turbulence, then the turbulence (and the associated fluctuations) are also expected to change smoothly.

3. Overview of the CO₂ diagnostic

Most of the measurements analysed in this paper were done using the LOTUS collective scattering diagnostic. This section gives a short overview of the device; a detailed description is published elsewhere [11].

The radiation source is a cw CO₂ laser, operated in the fundamental mode and yielding roughly 20 W. The laser beam is split into two parts by a Bragg cell: a high power main (M) beam and a low power local oscillator (LO) beam. In figure 3 the M beam is represented by a thick line, the LO beam by a thin line. The LO beam is frequency shifted by 40 MHz with respect to the M beam to enable heterodyne detection. The M and LO beams are crossed in the plasma, and light scattered from the M beam in the direction of the LO beam is detected.

The 'scattering angle' θ_s —the angle between the beams—selects the wavenumber $|\bar{k}_\perp| \equiv k_\perp$ according to

$$k_\perp \approx \frac{2\pi\theta_s}{\lambda_0}, \quad (1)$$

where $\lambda_0 = 10.59 \mu\text{m}$ is the wavelength of the laser radiation. The measurement volume is defined by the overlapping of the M and LO beams and has a vertical length $L_{\text{vol}} \sim 4w/\theta_s$. Here, w is the beam waist which is identical for the M and LO beams.

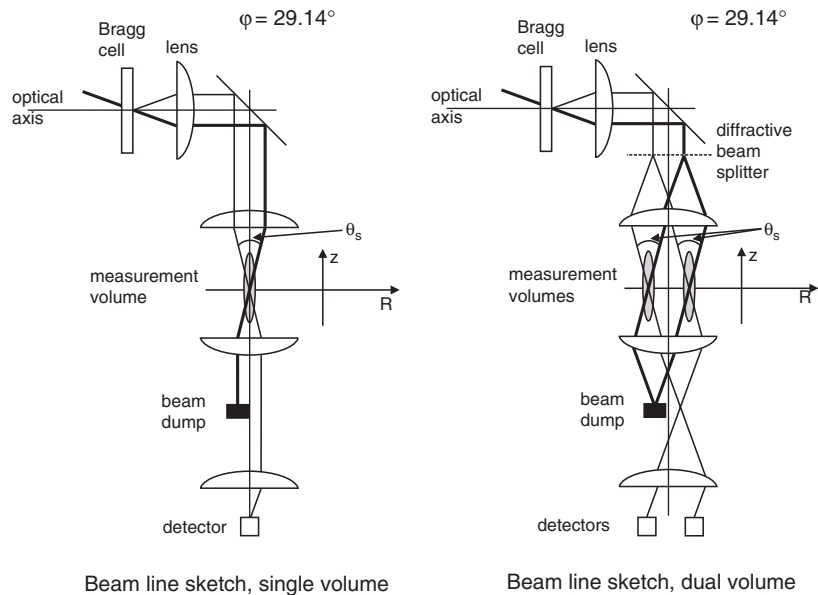


Figure 3. Schematic of the diagnostic setup: for the single volume setup (left) and the dual volume setup (right).

Usually the L_{vol} measurement volume is longer than the plasma itself; thus, the scattered power represents a line integral of the density fluctuations with a certain wavenumber along the scattering volume. The detector signal is quadrature demodulated to provide a complex signal; this way fluctuations travelling in the positive and negative k_{\perp} direction appear at negative or positive frequencies, respectively. The spectrum around 0 Hz is usually highly disturbed by mechanical vibrations; thus, fluctuations below 50 kHz are not analysed

To achieve some localization along the measurement volume, two approaches have been used: a single volume and a double volume one as shown in figure 3. The single volume localization relies on the experience that the wavevector of the density fluctuations is perpendicular to the local magnetic field [12]. By having a good wavenumber resolution and taking into account that the direction of the magnetic field changes along the scattering volume, one can achieve some vertical resolution. The two-volume localization uses a somewhat different assumption, namely that density fluctuations are highly correlated along the magnetic field, but have a relatively short correlation in the B_{\perp} direction. Both laser beams (LO and M) are split in two and two scattering volumes are formed. Crosspower of the signals from the two scattering volumes will contain fluctuations predominantly from those regions where the magnetic field passes through both scattering volumes. Selection of the position where the sensitivity is maximum is achieved by rotating the analysing wavenumber (single volume setup) or by rotating the two scattering volumes around an axis located between them.

The left-hand plot in figure 3 shows a single volume setup while the right-hand plot a dual volume one. For each of these, the scattered power (from one volume) can be written as

$$P(\alpha, \bar{k}_{\perp}) \propto \int_{z_b}^{z_t} \delta n^2(\bar{k}_{\perp}, z) \exp\left(-(\alpha - \theta_p(z)) \frac{N\pi}{2}\right)^2 dz, \quad (2)$$

where z is the vertical coordinate (along the measurement volume), α is the angle between the major radius R and \bar{k}_{\perp} (see figure 4), δn is the rms value of the density fluctuations, $\theta_p = \arctan(B_R(z)/B_{\phi}(z))$ is the horizontal pitch angle of the magnetic field and $N = 2w/\lambda_{\perp}$ is the fringe number [12].

For the single volume measurements, $\bar{k}_{\perp} = 15 \text{ cm}^{-1}$ and $w = 33 \text{ mm}$, while two setups were used for the dual volume setup: one where $w = 2 \text{ mm}$, the other for $w = 4 \text{ mm}$; \bar{k}_{\perp} was varied. The wide-beam waist in the single volume setup means that the diagnostic has a good wavenumber resolution. As the magnetic field changes along the observation volume

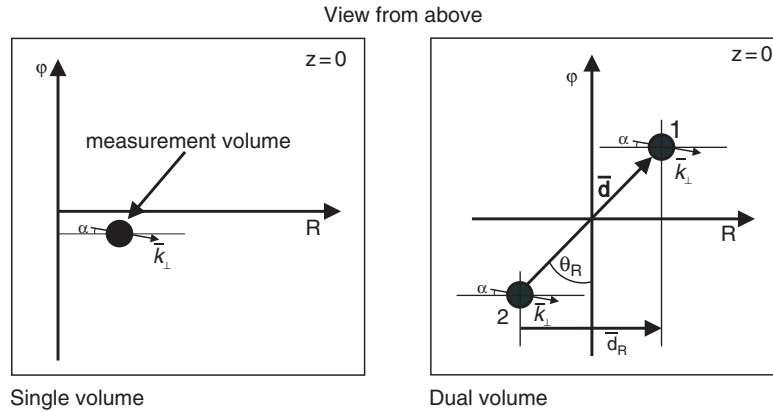


Figure 4. Top view in the equatorial plane of the stellarator of the single volume setup (left) and the dual volume setup (right). R is W7-AS major radius, ϕ is the toroidal direction.

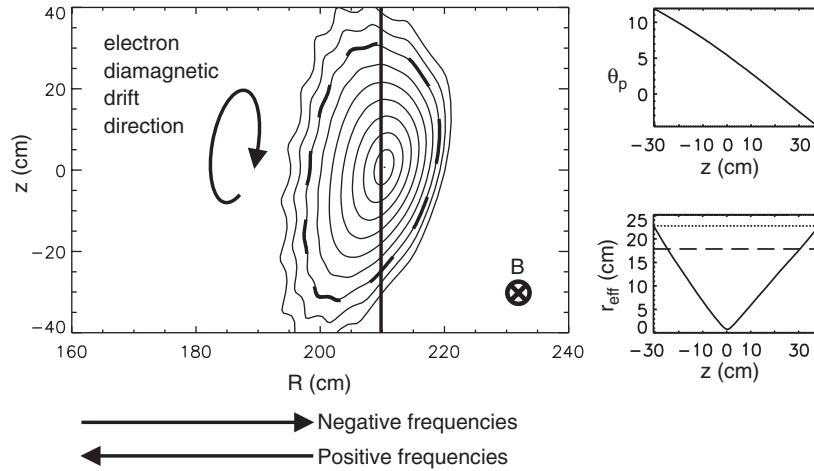


Figure 5. Flux surfaces at the diagnostic position (main figure), pitch angle along the vertical line (upper small inset) and the conversion between r_{eff} and z coordinates (lower small inset).

(see figure 5), equation (2) describes a somewhat localized sensitivity to density fluctuations. The regions where the magnetic field is directed perpendicular to the analysing wavevector will have maximum detection sensitivity. In the two-volume setup the wavelength sensitivity is much worse and localization is achieved by correlating the two (complex) detector signals. For a detailed analysis of crosscorrelation and crosspower functions, refer to [11].

To clarify the positional nomenclature, figure 4 shows a top view of the setups (looking along the beams) at $z = 0$ cm where the beams are focused and meet. From the left-hand figure (single volume), we see that the measured wavenumber is almost parallel to R , with a small deviation α . The angle α is remote controlled by stepper motors and can therefore be changed from shot-to-shot.

In contrast, the definitions necessary to describe the dual volume setup (right-hand figure) are somewhat more complicated: we again have a small angle α to describe the deviation from the R direction, but this is now fixed. However, in this type of setup the angle $\theta_R = \arcsin(d_R/d)$ is changeable from shot-to-shot. The distance d was kept at 14 or 29 mm.

Now that we have briefly described the diagnostic itself, figure 5 shows the centre of the single volume setup/centre of rotation for the dual volume setup on top of the flux surfaces (largest figure, $R = 209.8$ cm). We note that this vertical line passes almost exactly through the centre of the plasma. As we observe a horizontal wavenumber, $\bar{k}_\perp \equiv \bar{k}_r + \bar{k}_\theta \sim \bar{k}_\theta$, i.e. we measure the poloidal wavenumber. The dashed flux surface shows the last closed flux surface (LCFS) due to limiter action. For reference we also display the electron diamagnetic drift direction (clockwise) and the magnetic field direction. The arrows below the figure show the phase velocity direction of the fluctuations, giving rise to signals having positive and negative frequencies.

The upper small inset shows the magnetic field pitch angle in degrees as a function of the position along the vertical line representing the measurement volumes. The total variation of this angle is about 16° for the analysed discharge type.

The lower small inset shows the conversion between the z -coordinate and the effective minor radius coordinate r_{eff} . This effective coordinate enables mapping from diagnostics situated at different toroidal angles φ . LOTUS is positioned at $\varphi = 29.14^\circ$, which is close to the elliptical plane (at $\varphi = 36^\circ$). The long-dashed line shows r_{eff} at the LCFS, the short-dashed line shows the outer boundary of the plasma.

It has to be noted that most of the measurements presented in this paper were done using the two-beam setup. Only limited data are available from wide-beam measurements and due to the installation of the divertor into the W7-AS stellarator these measurements cannot be repeated.

4. Comparison of density fluctuations in good and bad confinement

This section presents the results of comparative investigations of density fluctuations in good and bad confinement plasmas. In most cases the bad confinement state was reached by a 2 kA current ramp, but for comparison currentless bad confinement discharges are analysed as well. The absolute sensitivity of the LOTUS diagnostic has not been calibrated so that our measurements give only relative changes in the magnitude of density fluctuations.

4.1. Changes in the wavenumber spectrum

The wavenumber spectrum of line integrated density fluctuations was analysed in the $k = 25\text{--}61\text{ cm}^{-1}$ range in a series of good and bad confinement discharges. The analysing wavenumber was changed from shot-to-shot, and measured power spectra were integrated for frequencies in the $(-1.5\text{ MHz}, 1.5\text{ MHz})$ band. The $(-40\text{ kHz}, 40\text{ kHz})$ band was omitted due to scattered light from the strong beam. Detection noise was determined from a time interval before the discharge and subtracted. Figure 6 compares spectra in two time ranges; one at 0.3–0.4 s before the current ramp, the second at 0.52–0.56 s when the diamagnetic signal is at minimum in the discharges shown in figure 1. The spectra are plotted both for good and bad confinement plasmas. One can see that in the initially good confinement discharge, the slope of the spectrum becomes steeper when the confinement deteriorates; at high k the fluctuation power drops about a factor of 3 while at $k = 25\text{ cm}^{-1}$ it is nearly unchanged. Similarly in the case of the static bad confinement discharge the slope of the wavenumber spectrum is steeper than in the good confinement discharge. In the initially bad confinement discharge the current ramp causes only a change in the amplitude and not a considerable change in the slope.

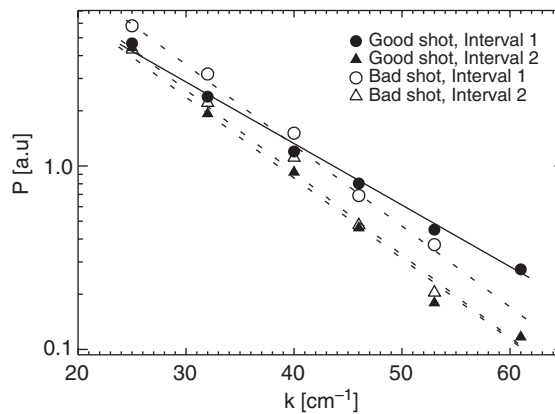


Figure 6. Wavenumber spectra of density fluctuations in good and bad confinement discharges before (interval 1) and during the current ramp when the diamagnetic signal in the good confinement discharge is at minimum (interval 2) (shots 45277–45288). The solid line represents the slope in good confinement (good shot, interval 1) and the dashed lines represent the slope in various bad confinement scenarios (good shot, interval 2 and bad shot).

During the current ramp the wavenumber spectra are very close to each other in the bad and good confinement discharges.

To see the temporal behaviour of the slope of the wavenumber spectrum, the spectra were calculated for 20 ms time windows in the fast current ramp discharge and fitted with a $P(k) = k^{-s}$ function. $P(k)$ is the fluctuation power at wavenumber k and s is the fitted exponent. The time evolution of the s exponent for both the good and bad confinement discharge is shown in figure 7. This figure clearly shows that the exponent changes differently for the two discharge types. For the bad confinement discharge the plasma current ramp causes a slight and gradual increase in the exponent. In the good confinement discharge the behaviour is more complex. When the current ramp starts at 0.4 s the exponent first decreases, later, when the confinement has minimum, it increases substantially and reaches about the same value as it is in the case of the bad confinement discharge. This way the change in the slope of the k -spectrum coincides with the change in plasma confinement: better confinement means smaller exponent. In other words the relative weight of the smaller wavenumbers (larger-scale structures) is higher if the confinement is worse.

The change in the slope of the wavenumber spectrum in figure 6 suggests that for $k < 25 \text{ cm}^{-1}$ there can be an increase of the fluctuation power in bad confinement. Therefore, in another setup of the diagnostic, measurements at $k = 15 \text{ cm}^{-1}$ were performed. These measurements cannot be combined into a single k -spectrum with the $k = 25\text{--}61 \text{ cm}^{-1}$ range, as the calibration of the diagnostic is different for different setups, but the time evolution of the relative fluctuation power can be analysed and compared to the higher k case. This is shown in figure 8. Indeed at $k = 15 \text{ cm}^{-1}$ the fluctuation power increases by about a factor of 2.

As we showed in figures 6 and 7, the shape of the k -spectrum during the current induced confinement degradation in the good confinement discharge becomes very similar to the bad confinement case. Figure 9 compares the power of density fluctuations for a good confinement discharge with slow current ramp (see figure 2) and the bad confinement $I_p = 0$ case at $k = 15 \text{ cm}^{-1}$. The result again shows that the current induced bad confinement is very similar to the discharge at the bad confinement t value. The fluctuation power at $k = 15 \text{ cm}^{-1}$ in the current induced confinement degradation coincides with that of the bad confinement discharge.

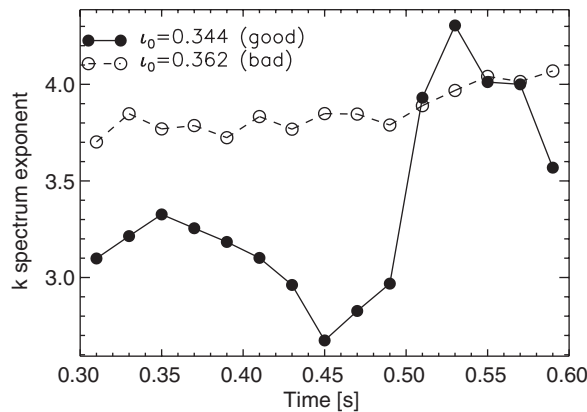


Figure 7. Change of the k -spectrum exponent vs time during the current ramp in good (●) and bad (○) discharges. The fluctuation power was averaged for the two channels. ι_0 is the initial edge rotational transform of the discharge before the current ramp (shots 45277–45288).

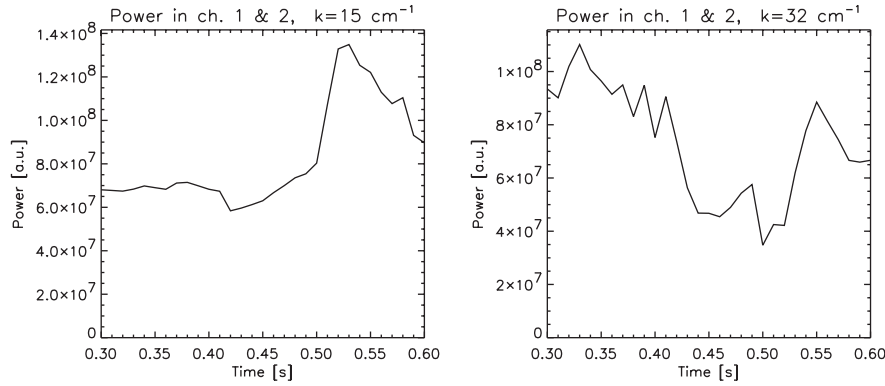


Figure 8. Change of the total fluctuation power averaged over the two channels vs time during a current ramp in a good confinement discharge. Left plot: $k = 15 \text{ cm}^{-1}$, right plot: $k = 32 \text{ cm}^{-1}$.

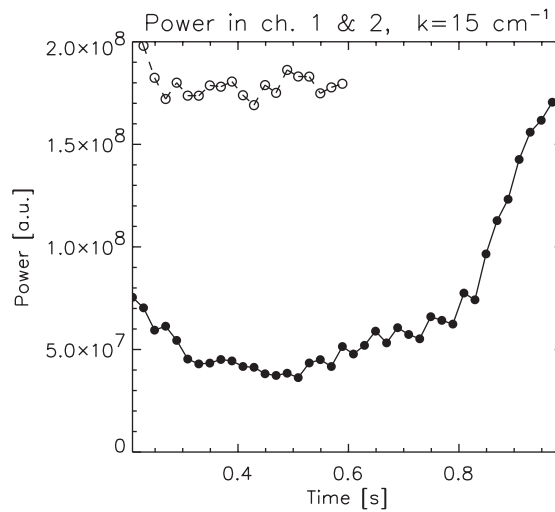


Figure 9. Temporal evolution of fluctuation power at $k = 15 \text{ cm}^{-1}$ during a slow current ramp discharge (47939, see figure 2) (●). For comparison a zero net current bad confinement (47945, shorter discharge) is shown with open circles.

4.2. Changes in the power spectrum

In section 4.1 the change in the frequency integrated density fluctuation power spectrum was analysed at different wavenumbers. Now we wish to investigate how the frequency spectrum behaves when the plasma confinement changes. Figure 10 shows the two-dimensional wavenumber–frequency spectrum of the density fluctuation power for ‘good confinement’ discharges in two time windows: before and on top of the current ramp. The $(-40, +40) \text{ kHz}$ frequency range is excluded from the figure as the signal in this band is dominated by leakage from the strong beam. The figure was compiled from a series of identical discharges where the CO_2 diagnostic measured at different wavenumbers. No $\omega(k)$ dispersion relation can be identified in the figure.

To better show the changes, power spectra at two k are plotted in figure 11 in initially good confinement discharges. In all of these plots the power spectra are compensated for

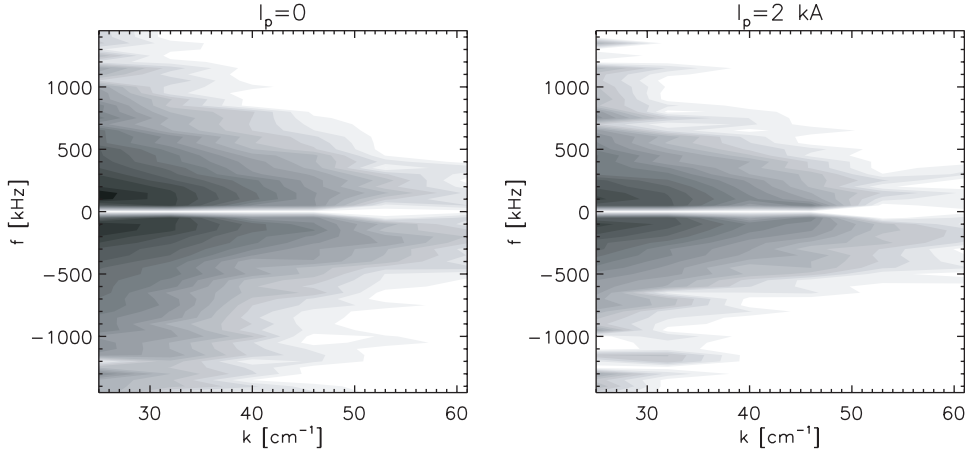


Figure 10. Wavenumber–frequency spectra of density fluctuations at $I_p = 0$ and on top of the current ramp ($I_p = 2$ kA) in good confinement discharges. The power scale is logarithmic.

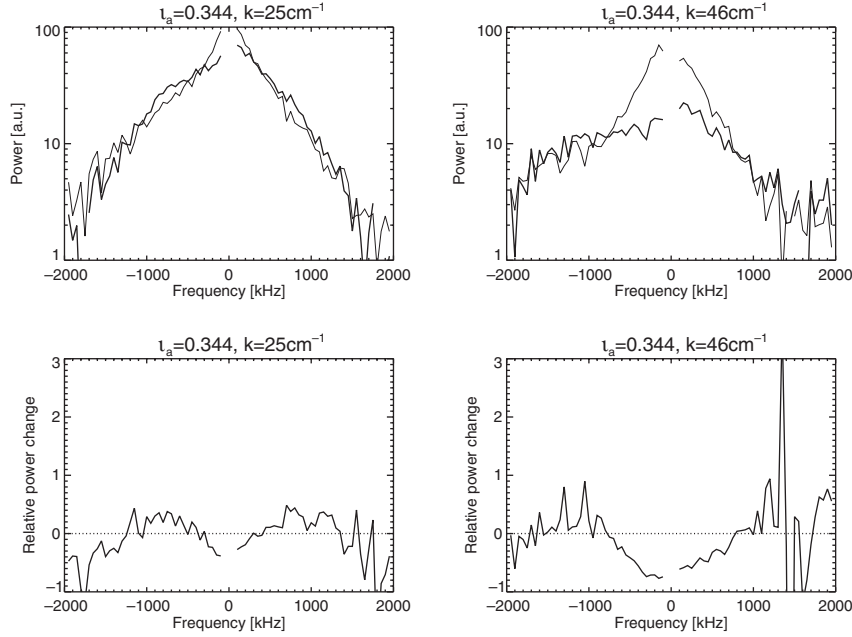


Figure 11. Frequency spectra of density fluctuations at $I_p = 0$ (—) and on top of the current ramp ($I_p = 2$ kA, ---) in good confinement discharges and the relative change of power (bottom). Left column: $k = 25$ cm $^{-1}$ (shot 45282), right column: $k = 46$ cm $^{-1}$ (shot 45278).

background detector and other instrumental noise sources by subtracting the power spectrum in a time window before the start of the discharge.

At $k = 46$ cm $^{-1}$ the drop experienced in the frequency integrated power (see figure 6) originates exclusively from the $(-500, 500)$ kHz band, no changes can be seen at higher frequencies. This tendency becomes even more pronounced at higher k . At $k = 25$ cm $^{-1}$ the drop in the $(-500, 500)$ kHz band is nearly compensated for by the increase at higher frequencies.

These power spectra can be compared to power spectra in bad confinement discharges plotted in figure 12. In these discharges the current ramp also causes some change in the power spectra, but the change is very similar at all k and frequency, a nearly uniform 0.2–0.3 times decrease is observed. The power spectra on top of the current ramp in initially good confinement discharges became similar to those of the bad confinement discharges.

It has to be noted that the power spectra in the $I_p = 0$ phase of the good confinement discharges seem to contain two features: a wideband spectrum and another one confined below 1 MHz. This is best seen at $k \geq 46 \text{ cm}^{-1}$. This low-frequency feature disappears on top of the current ramp in the good confinement discharges.

The power spectrum at $k = 15 \text{ cm}^{-1}$ (figure 13) where the density fluctuation power strongly increases on top of the current ramp in good confinement discharges (see figure 8)

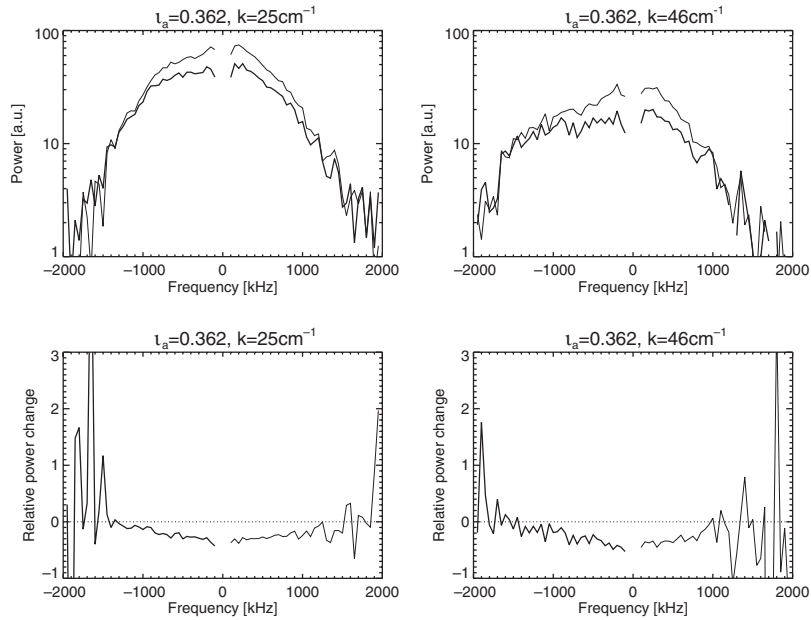


Figure 12. Frequency spectra of density fluctuations at $I_p = 0$ (—) and on top of the current ramp ($I_p = 2 \text{ kA}$, ---) in bad confinement discharges and the relative change of power (bottom). Left column: $k = 25 \text{ cm}^{-1}$ (shot 45283), right column: $k = 46 \text{ cm}^{-1}$ (shot 45286).

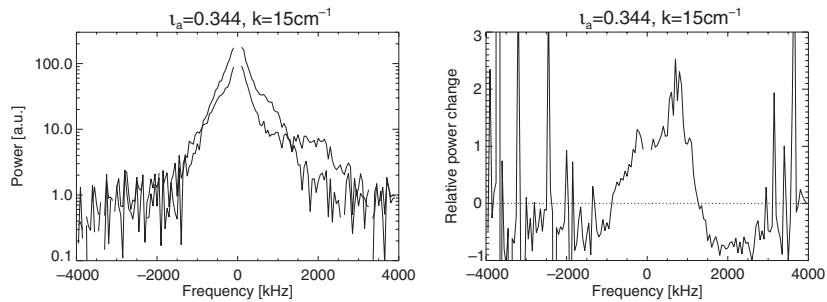


Figure 13. Frequency spectra of density fluctuations at $I_p = 0$ (—) and on left of the current ramp ($I_p = 2 \text{ kA}$, ---) at $k = 15 \text{ cm}^{-1}$ in a good confinement discharge (47933) and the relative change of power (right).

shows a different behaviour. In this case the measurable power spectrum extends to 3 MHz; thus it is plotted in the $(-4, 4)$ MHz band in figure 13. At this wavenumber the high-frequency feature is highly asymmetric in frequency and shows a frequency decrease when the plasma reaches bad confinement on top of the current ramp. An increase in power is observed up to 1 MHz frequency.

Summarizing the results of the power spectrum measurements, one can observe that there seems to be two phenomena present in the signals: a low-frequency (<1 MHz) and a high-frequency feature. The high-frequency feature appears to be symmetric in frequency and is unchanged at the confinement transition at $k = 25\text{--}60\text{ cm}^{-1}$. At $k = 15\text{ cm}^{-1}$ it has a highly asymmetric spectrum and a frequency decrease during the transition from good to bad confinement. The asymmetric shape might indicate that the fluctuations at $k = 15\text{ cm}^{-1}$ originate closer to the edge than the ones at higher k .

While the high-frequency feature shows a change during the confinement transition only at lower k , the low-frequency feature changes at all k . However, at $k = 15\text{ cm}^{-1}$ it exhibits an increase while at higher k it shows a drop in amplitude and even disappears at $k = 46\text{ cm}^{-1}$.

4.3. Radial profile of fluctuations

The power spectra represent line integrated measurements along the scattering beams; this way it is not possible to determine the radial profile of the fluctuations. However, some localization is possible with one of the techniques described in section 3. In sections 4.3.1 and 4.3.2 we describe the results with both techniques and then compare the results. The radial profile of density fluctuations was analysed at $k = 15\text{ cm}^{-1}$, where fluctuations increase in amplitude in the degraded confinement case.

4.3.1. Two-beam localization. Calculating crosspower spectra from the two measurement volumes, some localization can be achieved along the vertical chord as it is described in [11]. The essence of this localization is that the crosspower spectrum of the two measuring volumes selects those structures which are aligned along the line connecting the two volumes. As the structures in the turbulence are assumed to be aligned along the magnetic field lines, and the field lines change their direction along the vertical laser path, the crosspower spectrum shows only the fluctuations appearing at a certain vertical location. Due to the finite width of the scattering volumes and the finite cross-field correlation length of the structures, this localization is not perfect for the currently available 1–2 cm beam separation. Nevertheless, it was shown [11] that with this technique an up or down weighted power spectrum can be obtained.

Figure 14 shows the change in crosspower spectra (i.e. localized power spectra) at the bottom and at the top of the plasma when the plasma is moved from good to bad confinement. Top and bottom is selected by aligning the two scattering volumes to match the magnetic field direction at the top or the bottom of the plasma, respectively. First one observes that the negative and positive frequencies form two distinct spectra. More confirmation can be obtained for this fact from figures 19 and 20. A lower-frequency feature is present at negative frequencies at the bottom and positive frequencies at the top; thus it corresponds to poloidal flow velocity in the ion diamagnetic direction (*ion feature*). A higher-frequency *electron diamagnetic feature* is seen at the other side of the spectra. A strong up–down asymmetry can be observed in the two plots. At the bottom of the plasma, the frequency of the electron feature is considerably higher than at the top. This is probably a result of flux compression between the top and the bottom of the plasma as shown in figure 5. The magnetic surfaces are squeezed by about a factor of 2; thus the flow velocity should increase by the same factor to keep the flux constant in a volume element.

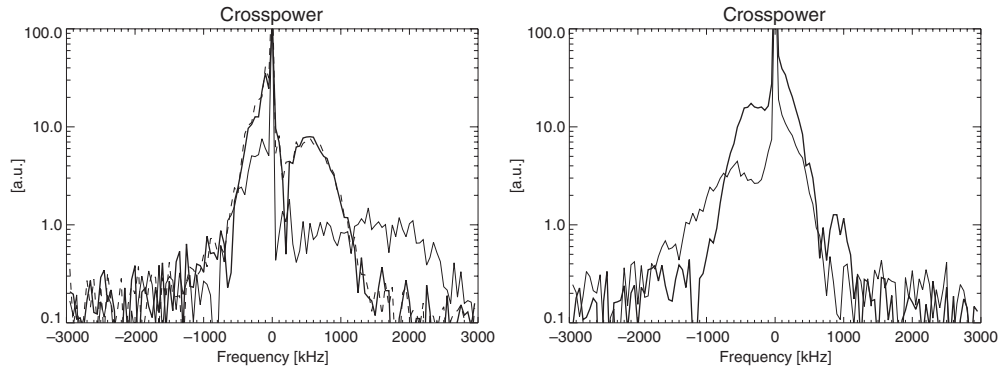


Figure 14. Crosspower spectra of density fluctuations at $k = 15 \text{ cm}^{-1}$ at $I_p = 0$ (—, shot 47943) and $I_p = 2 \text{ kA}$ (---, shot 47940) in a slow current ramp good confinement discharge. Volumes aligned along the magnetic field at the bottom (left) and at the top of the plasma (right). For reference a bad confinement $I_p = 0$ discharge is shown (····, shot 47946) on the left plot.

The power spectra in the current induced and static bad confinement plasmas are identical and significantly different from the good confinement case. The electron feature clearly changes its frequency by more than a factor of 2. In contrast to this, the frequency of the ion feature does not change significantly. The temporal evolution of this effect will be analysed in detail in section 5.

4.3.2. Wide-beam localization. In the preceding sections we have described both the line integrated measurements obtained from the dual volume setup and how one can achieve localization along the vertical chord using crosscorrelation techniques. This method is one of the methods which could be termed ‘indirect localization’, since it does not require the actual measurement volume size to be small. In this section we describe another indirect localization method, which requires a large fringe number N . This is realized by having a beam waist w which is considerably larger than the analysing wavelength λ_{\perp} . The method was first demonstrated by the ALTAIR team at the Tore Supra tokamak [12]. In contrast to the previous measurements, these are made using a single volume.

We made an α -scan (at 15 cm^{-1}) of the initially good confined ECRH plasmas as described in section 3: six identical shots were made, where α was set to the angles 12° (bottom), 8° , 6° , 4° , 0° and -4° (top).

Figure 15 shows the autopower for the six angles at good (thin line) and bad (thick line) confinement. The measurements were averaged over 50 ms. The central peak below $\pm 50 \text{ kHz}$ was cut. If we begin by commenting on the good confinement autopower spectra, it is clear that for the outermost measurement volumes (the upper left and lower right plots), two features are visible: one that dominates in amplitude is at low frequencies (100 kHz) and slopes outward; the other feature has a broader characteristic and the frequency sign (i.e. propagation direction) is opposite to that of the low-frequency feature. Referring to figure 5, we conclude that the high-amplitude, low-frequency fluctuations travel in the ion diamagnetic drift direction, while the low-amplitude, high-frequency feature travels in the electron diamagnetic drift direction.

As one moves further into the confined plasma, both features diminish and disappear almost completely in the core plasma. The radial resolution of the diagnostic makes it impossible to determine whether the radial range of the two counter-propagating features coincides or they are separated.

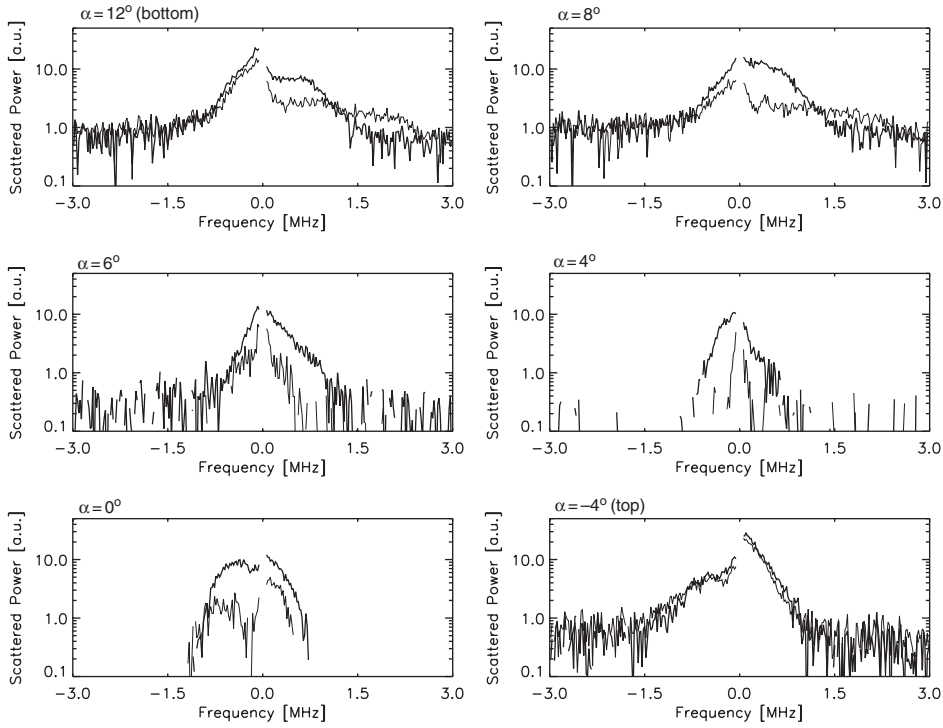


Figure 15. Autopower for the α -scan in a fast current ramp good confinement discharge. From top left to bottom right: $\alpha = 12^\circ$ (bottom), 8° , 6° , 4° , 0° and -4° (top). Thin lines are during good confinement, thick lines during bad confinement.

Let us now turn to the fluctuations during degraded confinement (thick lines in figure 15). Both the ion and the electron features increase their amplitude. In addition to this, the electron feature also decreases in frequency; it ‘spins down’. This observation is most clearly seen in the measurements of the fluctuations in the bottom of the plasma and confirms the crosspower amplitude results from the dual volume measurements in section 4.3.1.

Figure 15 showed two snapshots of the fluctuations at good and bad confinement. To display the changes in a more dynamical fashion, figure 16 shows contour plots of the density fluctuations at low frequencies. The traces above the contour plots show (from top to bottom) net plasma current (kA), gas fuelling (particles per second), stored plasma energy (kJ). The traces for all six shots are shown overlayed; note that they are very similar for the current and stored energy, meaning that the discharges (including the transition from good to bad confinement) are very reproducible. The traces on the left- and right-hand figure are identical and included above both figures for reference.

The contour plots in figure 16 show scattered power in black/white code vs time (horizontal axis) and plasma position in normalized coordinates (vertical axis): 1 corresponds to top position of the LCFS, 0 to centre and -1 to bottom LCFS. The time resolution was set to 10 ms. The left-hand plot shows the scattered power in the $(-120, -100)$ kHz band, the right-hand plot in the $(100, 120)$ kHz band. In the quiescent period (from 300 to 400 ms), the fluctuations do not change systematically in time. We again conclude that since the negative frequency fluctuations (left) dominate at the bottom while the positive frequencies (right) dominate at the top, these low-frequency fluctuations move in the ion diamagnetic drift direction. As the

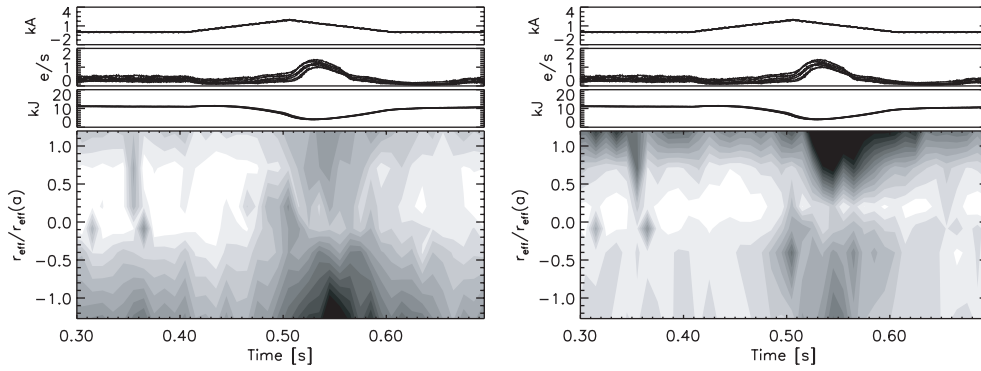


Figure 16. Traces of plasma quantities (net current, gas fuelling in units of 10^{21} and stored energy) and contour plots of density fluctuations in the $(-120, -100)$ kHz (left) and $(100, 120)$ kHz (right) frequency bands.

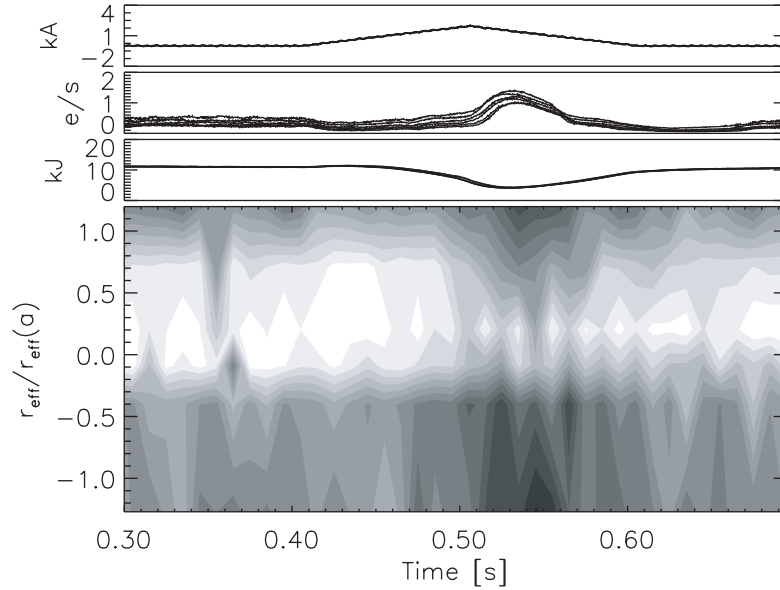


Figure 17. Traces (see figure 16) and contour plot of the density fluctuations integrated over all frequencies.

plasma enters the transient bad confinement phase, massive changes are observed in the density fluctuation profile: from being confined mostly to the edge plasma region, the fluctuations extend into the very core plasma during the degraded confinement phase.

Having seen the turbulence profiles for two frequency bands of opposite sign, it would, of course, be interesting to know how the ‘total’ (i.e. integrated over all frequencies in the $(-3, 3)$ MHz range, excluding $(-50, 50)$ kHz) turbulence profile behaves. This is displayed in figure 17. The same general behaviour is seen as in figure 16. Further, the fluctuations at the bottom seem to extend deeper into the plasma than the top fluctuations. This might be due to systematic errors in the calibration of the angle α (see discussion in connection to figure 18).

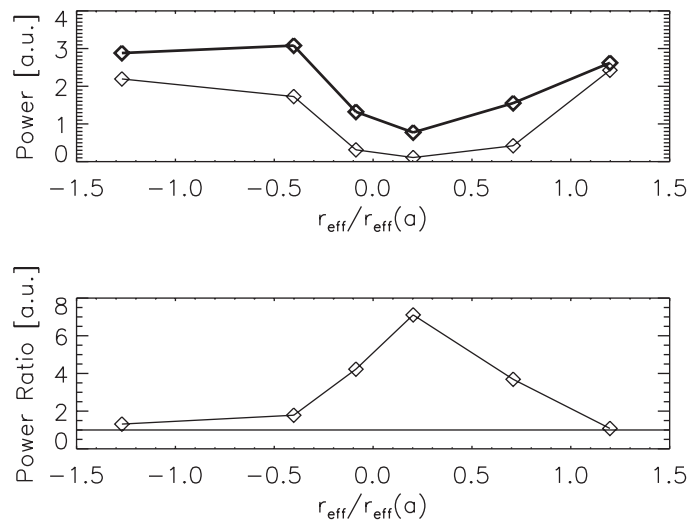


Figure 18. Density fluctuation power profiles—top: good confinement (—), bad confinement (—) and bottom: bad/good profile.

The final figure in this section, figure 18, shows the frequency integrated data of figure 15: the thin line shows the good confinement density fluctuation profile, the thick one shows the bad confinement profile. The plot at the bottom displays the ratio between the two. It is clear that the total fluctuation power increases most in the core, and if the peak in the ratio corresponds to the plasma centre, our calibration of α is not entirely correct.

4.3.3. Summary of the results from the two localization techniques. Although the two localization techniques have different radial resolution capabilities in the present setup, their results fit together very well. It can be stated that two features are clearly separated in the fluctuation: a wide band ($-2, 2$) MHz feature propagating in the electron diamagnetic direction and a lower-frequency ($-500, 500$) kHz feature propagating in ion diamagnetic direction.

Towards the plasma core the amplitude of both the ion and the electron feature strongly decreases. During the confinement degradation the electron feature at $k = 15 \text{ cm}^{-1}$ spins down, i.e. its frequency drops and both features increase in amplitude. The fluctuations extend from the edge plasma towards the centre. The largest relative fluctuation power increase is observed in the core plasma.

Table 1 summarizes the changes in density fluctuations when the plasma enters bad confinement either by changing the rotational transform externally or by an internal plasma current.

Table 1. Changes in density fluctuation at the good \rightarrow bad transition.

k -spectrum slope	$3 \rightarrow 4$
Amplitude @ $k = 15$	\uparrow
Amplitude @ $k = 46$	\downarrow
Poloidal flow velocity of electron	$\div 2$
d.d. feature @ $k = 15$	
Radial profile @ $k = 15$	Extends to core

5. The transition

All the results in section 4 indicate that the confinement degradation induced by a current ramp in a good confinement discharge at $t_a = 0.344$ results in a plasma state which is nearly identical to the bad confinement discharge at $t_a = 0.362$ with zero net current. It is also seen that the transition from good to bad confinement is not instantaneous. This leads to the idea to analyse the sequence of events which occurs when the plasma slowly goes from good to bad confinement. For this purpose slow current ramp discharges (figure 2) are used where current penetration is assumed to have less effect on the time evolution and the slow changes enable better resolution of the transition. (Calculations of the current profile evolution indeed indicate that the current penetration effect is negligible in these slow current ramp discharges.) As the CO_2 scattering diagnostic show that changes in fluctuation amplitude are the most pronounced at low wavenumber, we analyse $k = 15 \text{ cm}^{-1}$.

It has previously been shown that the fluctuations exhibit two phenomena: an electron and an ion feature. These two can be separated with one of the localization techniques described in section 3. For the slow current ramp discharges measurements with the two-beam technique were available. Figures 19 and 20 show the time evolution of power spectra of density fluctuations weighted towards the top and bottom of the plasma, respectively. (Top and bottom weighted power spectra are obtained by calculating crosspower spectra between the two measurement volumes aligned along the magnetic field lines on top and bottom of the plasma, respectively. For details see [11].) These figures exhibit a change in fluctuation characteristics associated with global confinement. Two phases can be clearly distinguished: (1) a gradual change occurs between 0.4 and 0.9 s; (2) saturation is reached at about 0.9 s. Although a gradual change is observed in the whole first time interval, the speed of the change clearly varies in time. A faster change both in amplitude and velocity is observed around 0.8 s, which correlates well with a faster change in the global plasma parameters in figure 2.

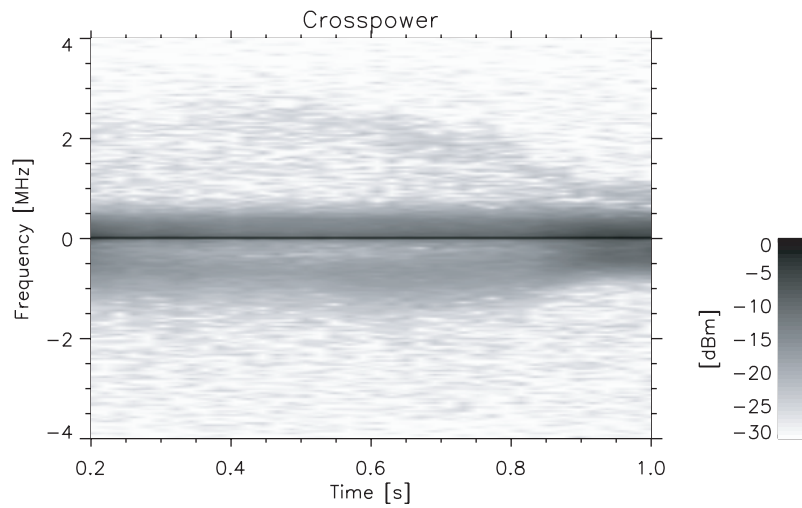


Figure 19. Time evolution of the crosspower spectrum in a slow current ramp discharge (see figure 2) when the scattering volumes are aligned along the magnetic field at the top of the plasma (shot 47937). The high positive frequency feature is most probably a crosstalk from the bottom of the plasma.

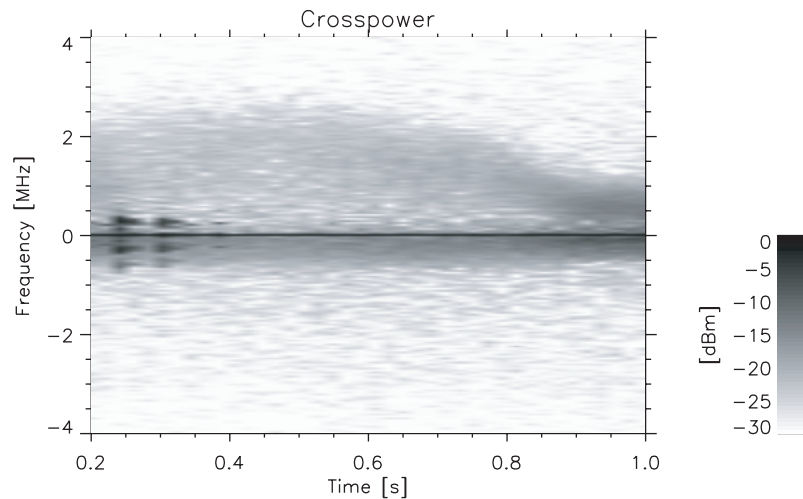


Figure 20. Time evolution of the crosspower spectrum in a slow current ramp discharge (see figure 2) when the scattering volumes are aligned along the magnetic field at the bottom of the plasma (shot 47940). The peaks in the spectrum between 0.2 and 0.3 s are due to instabilities in the laser.

In the first (gradual change) phase there is a clear gradual decrease in the frequency of the electron feature. The ion feature shows no change in frequency. In the second phase frequency spectra stay unchanged. The frequency drop is most probably an indication of a change in the poloidal flow velocity which occurs at the location of the electron feature. Although the radial electric field was not measured in the slow current ramp discharges, measurements on both the ‘good’ and ‘bad’ side of the ι edge are available in currentless discharges. These also show that the radial electric field at about $\frac{2}{3}$ of the minor radius is reduced by a factor of 2 in the bad confinement case.

The two phases are clearly identifiable in the diamagnetic signal of these types of discharges shown in figure 2 as well. It has to be noted that the saturation is preceded by a faster increase in the gas feed rate and a somewhat faster fall in the diamagnetic signal from about 0.8 s.

The two phases also appear if one plots the frequency integrated fluctuation power for the ion and the electron feature separately as it is shown in figure 21. These figures show the time evolution of the rms fluctuation power separately for the electron and the ion feature. Up to about 0.8 s there is only a moderate and gradual change in the power, but later on the increase is much faster. A clear saturation is not observed, but cannot be ruled out completely.

5.1. Magnetic field fluctuations

During the slow current ramp discharges, poloidal magnetic field fluctuations were also recorded using a set of 16 Mirnov coils [14]. Mode activity is often observed by this diagnostic. According to the Mirnov coil signal analysis these correspond to low m (2–4) poloidal perturbations with a short correlation time, typically only a few maxima and minima in the autocorrelation function [9, 14].

The amplitude of these waves is low, typically 10^{-5} T at the probe. Taking into account the poloidal size of the structures the magnetic field perturbation in the plasma can be considered to be on the order of 10^{-4} T, that is 1/1000-th of the poloidal magnetic field. In some low-density discharges analysed in [9] using BES, a density perturbation (≈ 3 –5%) correlated with these

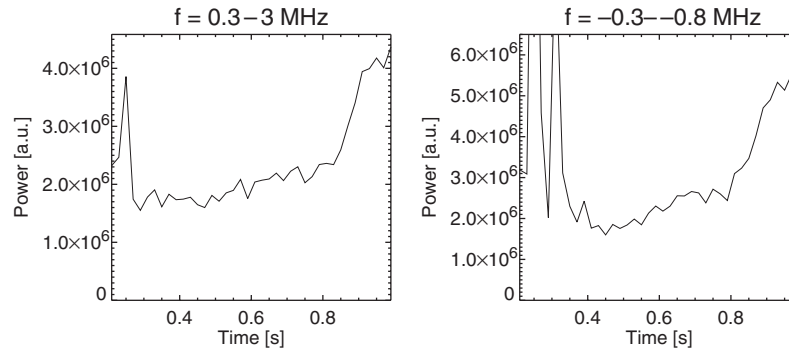


Figure 21. Time evolution of frequency integrated crosspower spectrum for the electron (left) and ion (right) feature during a slow current ramp discharge.

waves could be detected at the plasma edge. These observations showed that the perturbation extended only to maximum 2–3 cm radially and existed only inside the LCFS. It was also clearly shown that these waves could be switched on or off by changing the edge rotational transform without affecting the global plasma confinement.

Based on these observations we believe that these low-amplitude short-lifetime magneto hydrodynamic (MHD) waves do not cause significant transport but might represent the MHD response of the plasma to some transport events. For example when an eddy or other intermittent turbulent structure causes a fast rise or drop in the local plasma density, an MHD wave could be excited as a sound wave is excited by a hit on a bell. Of course, this mechanism will work only on rational surfaces which agrees with the observation that these fluctuations in the Mirnov signal are never correlated with scrape-off layer (SOL) density fluctuations. Given the radially localized appearance, we think that these phenomena can be used as markers of some (probably rational) surfaces in the plasma.

However, the quality of radial rotational transform calculations and the lack of localized fluctuation measurements in the core plasma make it hard to formulate quantitative relationships between the waves and the associated surfaces. Due to their low poloidal mode number these MHD fluctuations are not detected by the CO₂ laser scattering diagnostic and the BES measurement is usually limited to the edge plasma.

Figure 22 presents the time-dependent frequency spectrum of one Mirnov coil signal. The plot contains several distinct frequencies, initially at 20, 40, 60 and 110 kHz. During the current ramp the frequency of these modes (except the lowest frequency one) decreases, in agreement with the expectation that the flow velocity decreases. Interestingly at $t = 0.85$ s, the frequencies of the two lowest frequency modes coincide and the two lines merge. It has to be noted that this is the time when the diamagnetic signal drops faster than before and finally saturates. Also at the same time the amplitude of the density fluctuations starts to increase faster than before. A similar merge of two frequencies can be observed at 0.6 s between the 40 and 60 kHz mode.

Analysis of magnetic field fluctuations also show that between 0.8 and 0.9 s besides the frequency drop and narrowing of the spectrum the fluctuations become very much localized to a certain poloidal position in the cross-section of the Mirnov coils.

5.2. Edge density fluctuations

Edge density fluctuations were also recorded during the slow current ramp discharges with the accelerated Li-beam BES diagnostic [9]. The beam penetrates the plasma from the low-field

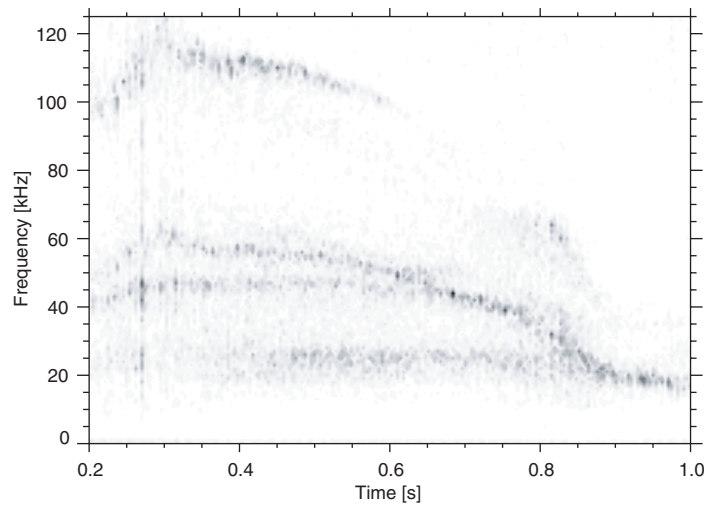


Figure 22. Time evolution of the frequency spectrum of poloidal magnetic field fluctuations during a slow current ramp discharge (shot 47940).

side (LFS). The fluctuations in this case are analysed in terms of correlation functions. Figure 23 shows the time evolution of autocorrelation functions of density fluctuations as grey scale coded plots at various places in the plasma. The distinct frequency modes seen in the magnetic field fluctuations would show up in this figure as periodicity (or at least peaks) in the vertical direction. One can observe that such structures can be found only inside the LCFS; in the SOL the autocorrelation function drops smoothly as a function of time lag.

The figure indicates, as it is generally found [9], that wave-like (quasi-periodic) fluctuations are present only in the confinement region and not in the SOL. Some frequencies seen in the Mirnov coil signal frequency analysis (figure 22) can be identified in the Li-beam BES measurements as well. The frequency of the lowermost stripe in the magnetic fluctuations is about 25 kHz which corresponds to $40 \mu\text{s}$ period time. This is clearly observed in the autocorrelation plot of Li-beam light fluctuations between 0.4 and 0.7 s with a slowly decreasing frequency. This frequency is observed only around the LCFS. The 40 kHz frequency (although its amplitude is higher in the magnetic signal) is not seen at the plasma edge; therefore, it is most probably located deeper in the plasma.

At about 0.7 s the clear mode structure disappears from the Li-beam signals. This is the time when the 40 kHz mode in the Mirnov signal starts to drop in frequency and interacts with the 25 kHz mode. At 0.75 s the 40 kHz mode appears in the Li-beam signal and clearly drops in frequency. As was previously speculated that this mode was deeper in the plasma; this way it moved radially, arrived at the edge at 0.75 s and interacted with the 25 kHz mode to finally form a single frequency. This time coincides with the time when both the gas feed rate of the discharge (figure 2) and the frequency integrated CO_2 scattering signals (figure 21) suddenly increase.

Finally at about 0.85 s all but a strong 20 kHz frequency disappears from the Mirnov signals. According to the Li-beam measurement this is localized about 4 cm deeper in the plasma than the original LCFS position. However, the density profile also shifts towards the machine centre; thus in the high-field side (HFS) the mode can be still located at the edge. (The Li-beam diagnostic is measured in the LFS.)

To show that the mode-like fluctuations measured by the Mirnov coils and the Li-beam are the same, the covariance (correlation without normalization) between a Li-beam light signal

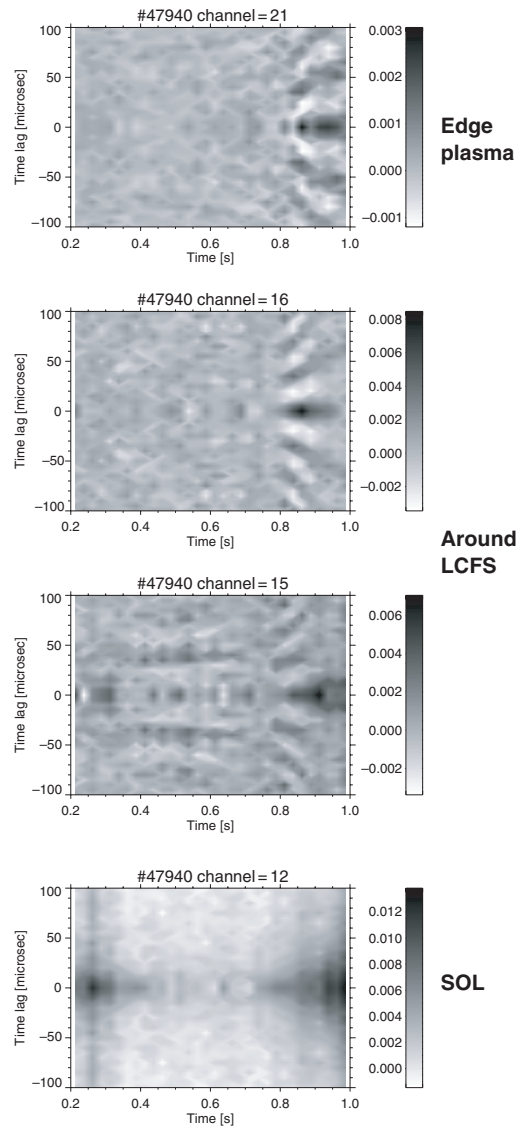


Figure 23. Time evolution of the autocovariance function of fluctuations in the Li-beam light in the SOL (bottom) around the LCFS (middle two figures) and in the edge plasma (top) during the slow current ramp measured by the accelerated Li-beam diagnostic.

and all the Mirnov coil signals in one toroidal cross-section is plotted in three different time windows in figure 24. Covariance is used instead of correlation to be able to investigate the amplitude distribution of the fluctuations in the Mirnov coil signals. For reference the mapping of the Li-beam along field lines to the cross-section of the coil system is shown.

The figure shows that a correlation indeed exists and it changes its character as the discharge moves through different phases. At 0.5 s a correlation is seen with all the coil signals with nearly identical amplitude. At 0.81 s an additional structure appears which is strongly localized to coils 8–11 which is the inboard side of the plasma where limiters are located. This feature shows a clear time delay between magnetic field and density fluctuations in the sense that

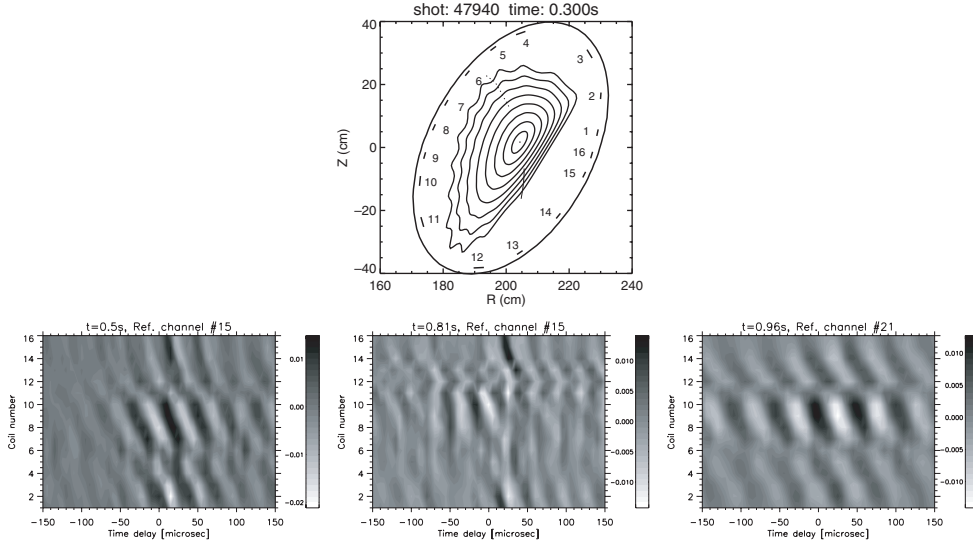


Figure 24. Covariance between a Li-beam channel and all of the Mirnov coils in one toroidal cross-section. The top figure shows the arrangement of the Mirnov coils and the plasma flux surfaces in the section of the Mirnov coil system. The radial lines show the mapping of the Li-beam along field lines to the position of the Mirnov coils. (Solid line: short connection, dashed line: long connection.)

magnetic field fluctuations around the limiter occur earlier than density fluctuations. It is important to observe that stronger correlation does not occur along the magnetic field lines connecting the coils and the Li-beam. In the third plot taken at 0.96 s, the strong 20 kHz fluctuation is observed in a correlated way in the Mirnov coil and Li-beam signals again with a strong localization at the inboard side.

5.3. Temperature profile changes

The behaviour of the electron temperature profile was analysed with the electron cyclotron emission (ECE) diagnostic. The time evolution of detection channels looking at the HFS is plotted in figure 25. These channels detect the electron cyclotron wave emission at fixed frequencies, i.e. the electron temperature is measured at certain magnetic field strengths. Due to the moderate change in the magnetic field during the current ramp, the spatial measurement position of the channels moderately shifts in time. Nevertheless, this shift is nearly uniform for all channels and the qualitative evolution of the temperature profile is clearly indicated. First one observes that at around 0.6–0.7 s three traces merge; thus a plateau forms in the profile. At around 0.8 s two more traces join this plateau. After 0.9 s saturation is seen, where the temperature profile becomes flat at a very low amplitude.

In order to give a general picture of the phenomena occurring during the slow current ramp induced confinement transition, table 2 summarizes the changes described in this section.

6. Discussion

The experimental results in the previous sections showed that not only global plasma confinement but electron density fluctuations change highly reproducibly during confinement

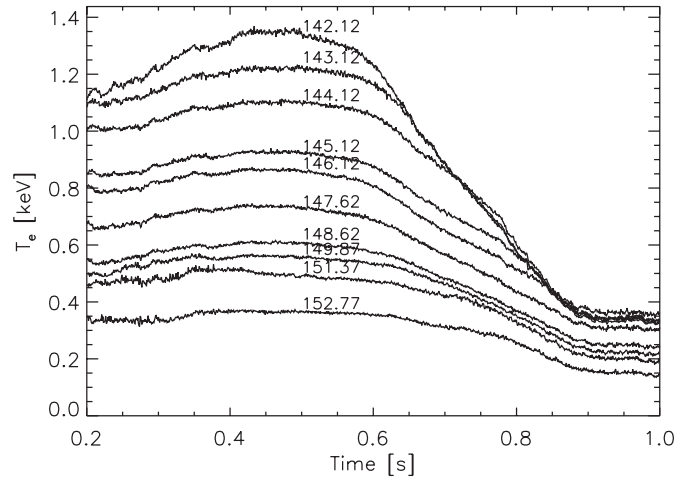


Figure 25. Time evolution of ECE traces at the HFS during the slow current ramp discharge. Although the spatial location where the channels measure shift in time due to the change in magnetic field, the relative profile evolution is clearly indicated. The numbers above the curves indicate the channel frequencies (GHz).

Table 2. Change in various quantities during the two phases of the confinement transition induced by a slow current ramp.

Quantity	Gradual phase (0.4–0.8 s)	Final phase (0.8–1.0 s)
Diamagnetic energy	Gradual decrease	Saturation at low level
Particle loss	Gradual increase	Fast increase, maximum
T_e profile	Plateau appears and gradually extends	Flat profile at low amplitude
Amplitude of electron d.d. feature @ $k = 15$	Gradual increase	Faster increase
Amplitude of ion d.d. feature @ $k = 15$	Gradual increase	Faster increase
Poloidal flow velocity of electron d.d. feature @ $k = 15$	Gradual decrease	Constant
Mirnov ‘modes’	Frequencies gradually merge	One strong 20 kHz mode
Mirnov amplitude profile	Distributed	Strongly localized to inboard equatorial plane
Edge density fluctuations	Modes slow-down	One strong 20 kHz mode
SOL density fluctuations	No obvious change	Strong increase

transitions induced in the W7-AS stellarator either by changing the externally applied rotational transform or by inducing an Ohmic plasma current in the plasma [5]. With this latter method the temporal evolution of the transition can also be investigated. It was shown that the transition time is determined by the current ramping time and not by the internal dynamics of the transition. This observation excludes that some positive feedback mechanism acts in the transition and this behaviour is in clear contrast to H-mode transition [10]. The changes analysed in this paper are completely steerable by the magnetic configuration. Transitions induced by external fields and by internal plasma currents caused the same change in both the wavenumber and frequency spectra of electron density fluctuations.

Wavenumber spectra in the $25\text{--}60\text{ cm}^{-1}$ range show a clear steepening when the plasma goes into a degraded state, the relative weight of larger structures increases. The rms fluctuation amplitude at a fixed wavenumber can show either positive or negative correlation with the confinement quality. At large k (small structure size) the amplitude clearly drops, while at low k ($<25\text{ cm}^{-1}$) the amplitude increases. These observations indicate that if the confinement transition is caused by turbulence, the role of wavenumbers below 25 cm^{-1} should be important.

Frequency spectra show two distinct phenomena both in the good and bad confinement state: a lower frequency ($<500\text{ kHz}$) one propagating in the ion diamagnetic drift direction and a higher frequency one ($<3\text{ MHz}$) moving in the electron diamagnetic direction. Although the radial extent of these two features is unclear, from electric field measurements and results from other machines probably the ion feature is located closer to the plasma edge. If the density fluctuations are convected along the $\mathbf{E} \times \mathbf{B}$ flow, this observation would be consistent with an inversion of the radial electric field E_r with a negative E_r inside the LCFS and a positive E_r outside the inversion layer. This has indeed been confirmed in most toroidal confinement devices, including W7-AS [13].

Although the CO₂ diagnostic measures a line integral of the rms density fluctuation amplitude, two techniques have been applied to get a limited radial resolution. It was shown that the $k = 15\text{ cm}^{-1}$ density fluctuations, limited to the edge in the good confinement state, extend into the plasma core in the bad confinement state.

The sequence of events during the good to bad confinement transition was analysed by a slow current ramp, in which current penetration effects do not play a significant role and the transition takes places in more than 10 times the energy confinement time. The most obvious event observed by the CO₂ laser scattering diagnostic is a gradual decrease in the poloidal flow velocity of the fluctuations moving in the electron diamagnetic direction and a saturation when the confinement saturates at a low level. The same slow-down is not seen for the fluctuations moving in the ion d.d. direction. This fact was confirmed by reflectometry measurements as well. Spectroscopic radial electric field measurements in fast current ramp discharges also agree in the direction and approximate magnitude of the change. It is not clear whether this is a cause or a result of the confinement degradation. Density and temperature profile measurements indicate that in the first part of the transition the electron temperature profile degrades and the density and gas feed rate is nearly unchanged. Consequently the confinement degradation affects first the electron confinement which clearly changes the radial electric field distribution and consequently the poloidal flow velocity. Reasoning in the other way one could assume an effect of the flow velocity reduction on the confinement quality through reduction of the shearing rate. For such an explanation one would need an effect which changes the flow velocity as a function of edge rotational transform. Even if this is assumed the positive feedback from the confinement change (as considered in case of the H-mode transition) back to the flow velocity is clearly nonexistent in our case as the transition is externally controllable.

It was shown from magnetic field fluctuation measurements that short correlation time ($\approx 100\text{ }\mu\text{s}$) mode-like fluctuations are also present in the plasma. These are known to have a poloidal mode number $\text{int}(1/\iota)$ [14] and are thus not directly observable by the CO₂ laser scattering diagnostic. It is known that the presence of these modes at the plasma edge is very sensitive to the edge ι [9]. In the slow transition (slow current ramp) discharges, several of these modes could be detected at the same time. Their frequency is also seen to decrease gradually in agreement with the idea of a gradual slow-down of the poloidal flow velocity. Due to the low shear of the W7-AS plasma it is unlikely that the difference in the poloidal mode number causes the difference in frequencies. It is expected that different frequencies

correspond to different poloidal flow velocities at different radial positions. (It has to be noted that due to the lack of axial symmetry, the flow velocity in the W7-AS stellarator is expected to be predominantly poloidal.)

This is also supported by the fact that the mode frequencies merge smoothly which would not be possible in case the poloidal mode numbers were different. (This might not apply for the highest frequency mode at 110 kHz which might correspond to another poloidal mode number than the other three modes.)

Although the origin of these modes is not clear, they are most probably localized to certain ι values (probably to rational surfaces or close to rational surfaces) and this way they constitute some kind of ‘marker’ for these surfaces. The present diagnostic and computational capabilities do not allow us to identify the exact value and location of the surfaces in question. Nevertheless, their transformation and appearance at the plasma edge (as seen by the high-energy Li-beam diagnostic) show interesting correlation with plasma confinement. During the gradually changing phase of the slow transition discharge, one of the modes is seen around the LCFS, other modes are localized deeper in the plasma. During the gradual confinement degradation two of the modes inside the plasma merge in frequency approximately at the same time when a plateau in the electron temperature profile is formed. Later in the discharge the mode which was originally localized deep in the plasma appears at the edge and merges in frequency with the originally present edge mode. This occurs at the same time when the particle loss from the plasma increases (the gas feed rate for keeping the line density constant increases), and the density fluctuation amplitude starts to increase faster than before. The electron temperature profile also shows an extension of the plateau at the same time. Finally, the confinement saturates at a low level and the magnetic and edge density fluctuations are dominated by a single strong mode. The poloidal distribution of the magnetic fluctuations is strongly localized at the inboard equatorial plane. As limiters are located in each module of W7-AS, at this place a strong interaction between the mode and the limiter is probable [15].

Using the above considerations, merging of two frequency lines in figure 22 could be an indication of the formation of a plateau in the radial profile of the poloidal flow velocity between the two corresponding rational surfaces on which the associated poloidal mode numbers are equal, e.g. $m/n = 3/9$ and $3/10$ modes. Such plateau formation is clearly observed in the ECE temperature profiles and changes in the plateau width seem to correlate with timepoints where two Mirnov frequencies merge. This effect might even be more accelerated if the two neighbouring modes would interact and phase lock.

The observations presented in the previous sections can be qualitatively understood on the basis of the phenomenological model of the confinement transitions described in [5]. In the good confinement case the plasma is composed of radial zones of good and bad confinement. The alternation of these zones is governed by the radial ι profile. Short-lifetime mode-like oscillations randomly appear in some (probably the bad confinement) zones. The presence of many different frequency modes in the plasma indicates a series of different flow velocity zones separated by good confinement layers. During the gradual change in ι profile these zones shift and change their radial extension. At a certain point two zones merge, forming a plateau in electron temperature and merging of two mode frequencies in the magnetic fluctuations. The extension and movement of the zones cause an increase in the line integrated density fluctuation amplitude. At a later timepoint, the remaining bad confinement zones merge, forming a large zone which extends to the plasma edge and interacts with the limiter. This causes a strongly degraded plasma state. Due to the direct interaction between the SOL and the confinement region, the plasma density fluctuation amplitude and particle loss increase substantially.

7. Conclusion

The experimental results presented in this paper show a clear correspondence between plasma fluctuations, confinement and rotational transform. Confinement degradation is accompanied by the buildup of mm scale structures in the density fluctuation. Several short correlation time mode-like fluctuations are seen to be present in the plasma with different frequencies. The location of these modes clearly changes when the edge rotational transform is changed; thus, they are connected to certain values of ι . It is shown that confinement quality and fluctuations change considerably when such modes merge in frequency or arrive at the plasma edge. Although a slow-down of the poloidal flow velocity is also observed during the confinement degradation, it can be understood as a result of the change in the ambipolar radial electric field. It is thus unlikely that confinement changes would be caused by shearing of the turbulent structures.

Acknowledgments

The authors thank R Brakel and J Baldzuhn for detailed discussions. Technical support for the CO₂ scattering diagnostic by H E Larsen, B O Sass and J C Thorsen from Risø and H Scholz from IPP is acknowledged. The hospitality and active support of the whole W7-AS Team is greatly contributed to achieving the results described in this paper.

References

- [1] de Baar M R *et al* 1999 *Phys. Plasmas* **6** 4645
- [2] Schüller F C *et al* 2000 *27th EPS Conf. Control. Fusion and Plasma Phys. (ECA)* vol 24B, p 1697
- [3] Cardozo N J L *et al* 1997 *Plasma Phys. Control. Fusion* **39** B303
- [4] Renner H *et al* 1989 *Plasma Phys. Control. Fusion* **31** 1579
- [5] Brakel R *et al* 1997 *Plasma Phys. Control. Fusion* **39** B273
Brakel R *et al* 1998 *J. Plasma Fusion Res.* **1** 80
- [6] Brakel R *et al* 1998 *25th EPS Conf. Control. Fusion and Plasma Phys. (ECA)* vol 22C, p 423
Brakel R *et al* 1999 *12th International Stellarator Workshop (Madison Wisconsin)*
- [7] Liewer P C 1985 *Nucl. Fusion* **25** 543
- [8] Wootton A J *et al* 1990 *Phys. Fluids B* **2** 2879
- [9] Zoletnik S *et al* 1999 *Phys. Plasmas* **6** 4239
- [10] Erckmann V *et al* 1993 *Phys. Rev. Lett.* **70** 2086
- [11] Saffman M *et al* 2001 *Rev. Sci. Instrum.* **72** 2579
- [12] Truc A *et al* 1992 *Rev. Sci. Instrum.* **63** 3716
- [13] Baldzuhn J *et al* 1998 *Plasma Phys. Control. Fusion* **40** 967
- [14] Anton M *et al* 1998 *J. Plasma Fusion Res.* **1** 259
- [15] Fenzi C *et al* 2000 *Nucl. Fusion* **40** 1621